ChemComm
Chemical Communications

Accepted Manuscript

This article can be cited before page numbers have been issued, to do this please use: S. R. Mangu and V. Chakrapani, *Chem. Commun.*, 2026, DOI: 10.1039/D6CC01794K.

ROYAL SOCIETY OF CHEMISTRY

rsc.li/chemcomm

ChemComm

View Article Online
DOI: 10.1039/D6CC01794K

COMMUNICATION

Dual Role of Azide as a Quencher and Stimulator of Singlet Oxygen Generation on Some Manganese Oxides

Shashank Mangu,[a] and Vidhya Chakrapani [a,#]

Received 00th January 20xx,
Accepted 00th January 20xx

DOI: 10.1039/x0xx00000x

Sodium azide is a known singlet oxygen ($^1O_2$) quencher in both homogenous and heterogeneous catalytic transformations. We report a paradoxical trend of a strong enhancement in the $^1O_2$ production during H_2O_2 disproportionation seen on some MnO_x catalyst, specifically layered δ-MnO_2. Studies with $^1O_2$-specific probes show that this activation is due to N_3^- complexation with lattice Mn^{II} of δ-MnO_2 that upon rapid air oxidation produces a metastable surface Mn^{III}-azide complex that strongly catalyzes H_2O_2 disproportionation. In contrast, a bulk Mn^{III}-azide complex does not produce $^1O_2$. Due to this dual role, the use of NaN_3 as diagnostic tool for $^1O_2$ intermediacy should be carefully reconsidered.

Singlet oxygen ($^1O_2$) is a nonradical reactive oxygen species (ROS) known for its high specificity for electrophilic compounds, including biomolecules such as nucleic acids, lipids and proteins, and is exploited in several industrial transformations. A major diagnostic tool for detecting the presence of $^1O_2$ in aqueous media is using chemicals traps and quenchers. For example, reactive dienes, such as 9,10-disubstituted anthracene, are commonly used traps that selectively react with $^1O_2$ to form stable endoperoxide adducts that can be detected by mass spectroscopy.[1] In this process, the traps are consumed depending on the rate of $^1O_2$ formation. On the other hand, physical quenchers that deactivates $^1O_2$ to triplet oxygen ($^3O_2$) through a radiationless process are the most preferred probes for $^1O_2$ since the quencher is not consumed and no new products are formed that can contaminate the product stream. Sodium azide (NaN_3) is the most used physical quencher, often used to monitor the presence of $^1O_2$. The deactivation process is given:[2, 3]

$$^1O_2 + N_3^- \rightarrow {}^3O_2 + N_3^- \qquad \textbf{Reaction 1}$$

$$O_2 + N_3^- \rightarrow {}^1\left(O_2^{-*}\cdots N_3^*\right) \xrightarrow{ISC} {}^3\left(O_2^{-*}\cdots N_3^*\right) \rightarrow O_2^{-*} + N_3^* \rightarrow {}^3O_2 + N_3^- \qquad \textbf{Reaction 2}$$

The rate constant for **Reaction 1** is high with a measured value of 5.0 X 10^8 $M^{-1}s^{-1}$ in water.[4] The accepted quenching mechanism obtained from electron spin resonance (ESR) studies is that it proceeds through the formation of a singlet charge transfer complex (**Reaction 2**) in which the electronic charge of N_3^- is partially transferred to oxygen leading to the formation of radical intermediates of superoxide (O_2^{-*}) and azidyl (N_3^*).[2] This complex undergoes intersystem crossing (ISC) to the triplet ground state with the release of energy (heat) and then dissociates to triplet oxygen ($^3O_2$) with the regeneration of azide anion. Several factors are known to affect this interactive bimolecular quenching rate for the process in homogeneous and heterogeneous systems, such as viscosity[5], dielectric constant (polarity)[5], temperature,[6] ionic strength of the protic solvents,[7] and the degree of protonation of azide.[4] Other electron-rich quenching agents, such as amines, also follow this mechanism for $^1O_2$. Herein we show that NaN_3 is not a quencher for $^1O_2$ produced by some MnO_x, specifically δ-MnO_2 containing a high concentration of lattice Mn^{II}. Rather, the presence of N_3^- ions enhance $^1O_2$ production through the formation of Mn^{III}-azide complex that is highly catalytic towards H_2O_2 disproportionation.

We performed tests with several Mn and non-Mn based oxide catalysts that were otherwise efficient $^1O_2$ generators in the absence of azide. These include stoichiometric V_2O_5, δ-MnO_2, acid treated hexagonal δ-MnO_2 (H-δ-MnO_2), $(La_{0.8}Sr_{0.2})_{0.95}MnO_{3-\delta}$ (henceforth LaSrMnO$_3$), $LiMn_2O_4$, and La_2NiO_4.[8] Two $^1O_2$-sensitive fluorogenic probes were used: 1,3 diphenylbenzofuran (DPBF) and singlet oxygen sensor green (SOSG). DPBF is the most used and well-characterized $^1O_2$ probe due to its high fidelity against $^1O_2$ photosensitization. It strongly absorbs light at ~410 nm and emits bright blue fluorescence (~480 nm) that is proportionally quenched when it reacts with $^1O_2$ to form an endoperoxide or 1,2-dibenzoylbenzene that is not fluorescent. The rate constant for this reaction is high, with a value of 2.3 x10^9 $M^{-1}s^{-1}$ in an ethanol / water (50/50 v/v) mixture[9]. In a typical run, 1 mg of catalyst was first incubated with 30 µM of probe along with NaN_3 (if present) to achieve stable coverage and then reacted with 10-40 µM of H_2O_2. The emission intensity of the supernatant only after centrifugation was measured. While a decrease in the DPBF intensity is indicative of extent of $^1O_2$ generation, a decrease can also be caused by the removal of DPBF molecules from the solution due to its adsorption

[a] Howard P. Isermann Department of Chemical and Biological Engineering
Rensselaer Polytechnic Institute, Troy, NY-12180
[b] # Email: chakrv@rpi.edu.

View Article Online
DOI: 10.1039/D6CC01794K

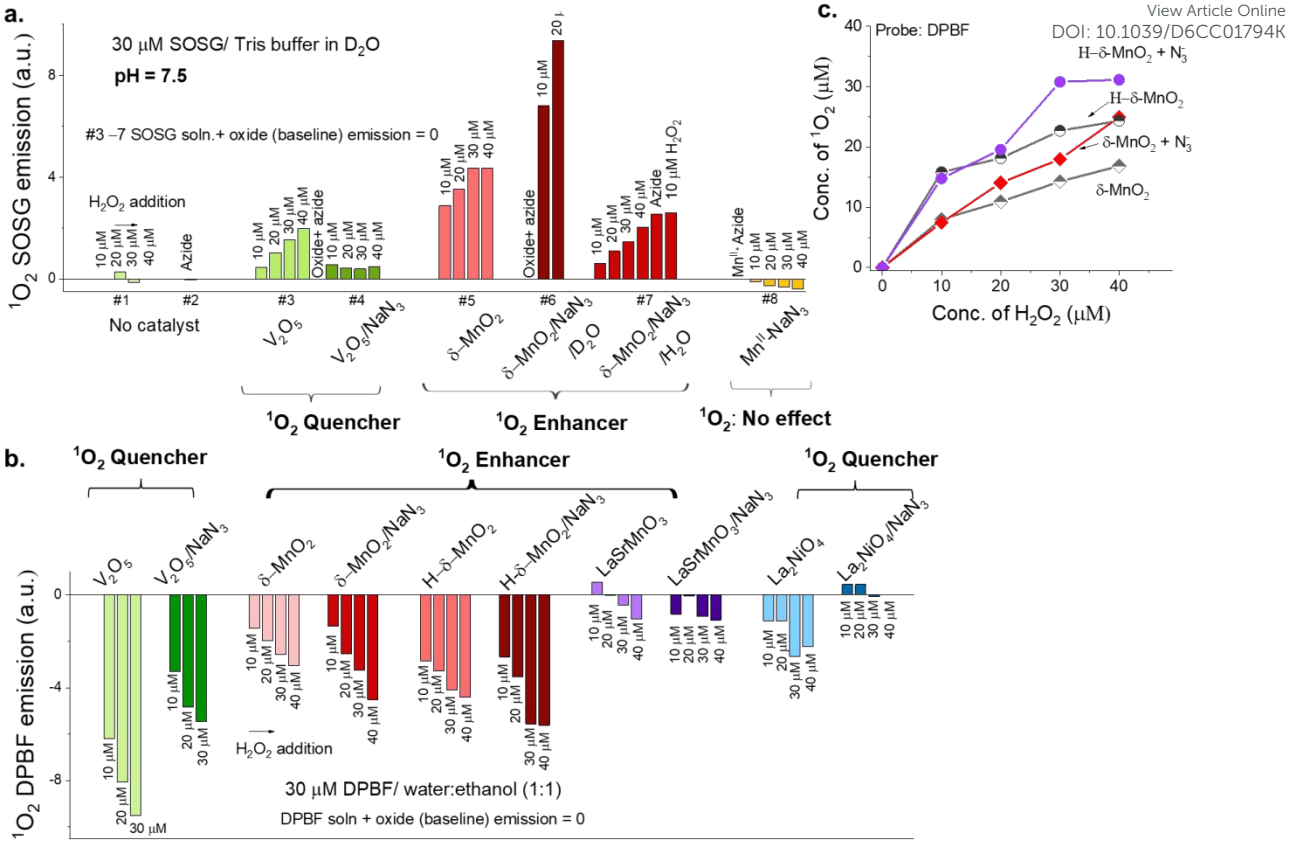

Figure 1. *Contrasting trends in $^1O_2$-related SOSG (a) and DPBF (b) emissions as well as $^1O_2$ production (c) caused by the presence of NaN_3 in the electrolyte exposed to V_2O_5, δ-MnO_2, and other oxide powders in the presence of 10-40 μM H_2O_2 concentrations. Also shown is the effect of H_2O_2 addition to the bulk Mn^{III}-azide complex. Oxide weight = 1 mg/ml. [NaN_3] = 15 mM.*

on the catalyst. Therefore, for incontrovertible evidence for $^1O_2$ production, we used a second probe, SOSG, which shows a positive increase in emission, unlike DPBF that shows an emission decrease, upon reaction with $^1O_2$. In this case, any SOSG adsorption on the catalyst surface will only lead to a decrease and not an increase in the emission intensity. SOSG is made up of a fluorescein-type fluorophore and an anthracene-derived trapping moiety. In the absence of $^1O_2$, the fluorophore's emission of the fluorophore is quenched by internal transfer from the anthracene moiety. However, after the reaction of the anthracene moiety with $^1O_2$, which forms an endoperoxide that is no longer an efficient intramolecular electron donor, the fluorescence of the fluorophore is restored in proportion to the concentration of $^1O_2$. Furthermore, SOSG is also insensitive to ROS such as OH^* or O_2^{-*} and has a high fidelity unless when exposed to UV radiation.[10, 11] All SOSG tests were done with non-UV excitation wavelength of 405 nm in 0.1 M Tris buffer made with D_2O or H_2O. DPBF tests were performed in a 1:1 (v/v) ethanol/water mixture due to its limited solubility in water.

Initial tests of N_3^- effect on the $^1O_2$ production were performed with V_2O_5 and δ-MnO_2 as catalysts. V_2O_5 was chosen because it is known to disproportionate H_2O_2 to $^1O_2$.[12] Single-crystalline V_2O_5 nanostructures were grown using hot filament chemical vapor deposition process.[13, 14] δ-MnO_2 was prepared by wet precipitation of $KMnO_4$ solution using HCl. **Figure 1a** shows the change in the emission intensity of $^1O_2$-sensitive SOSG solution. The baseline emission of the supernatant without any H_2O_2 was taken as zero. One observes that for both oxides in the absence of N_3^-, the SOSG emission increases with increasing H_2O_2 concentrations (test #3 and #5), with δ-MnO_2 displaying higher activity for $^1O_2$ generation than V_2O_5. In the presence of N_3^-, contrasting trends are observed. In V_2O_5, the presence of N_3^-, which was added prior to the addition of H_2O_2, caused significant quenching of the $^1O_2$ signal (test #4), which decreased by 75% with the addition of 15 mM of NaN_3 compared to case without N_3^-. This is as expected and indicates that N_3^- act as a $^1O_2$ quencher. In contrast, the addition of H_2O_2 to azide-containing buffer with δ-MnO_2 led to a dramatic increase of $^1O_2$ signal by 120% (test #6), compared to the same test without azide. This suggests that N_3^- induces $^1O_2$ production in δ-MnO_2. Note that neither N_3^- nor H_2O_2 alone in the absence of oxide catalyst cause any change in the emission intensity of the probe (test #1 and #2). This shows the N_3^-- stimulated $^1O_2$ generation seen with δ-MnO_2 is not due to reaction with the probe. The $^1O_2$ generation was confirmed using D_2O/H_2O isotope effect. The lifetime of $^1O_2$ in H_2O is only 2.5 μs but increases nearly 10 times (~20 μs) in D_2O.[15, 16] The solvent-induced quenching of $^1O_2$ is most efficient when the infrared vibrational frequencies of the solvent (*e.g.* H_2O) coincide with the energy of $^1\Delta \rightarrow {}^3\Sigma$ transition of O_2, thus causing deactivation by transferring the correct quanta of energy. [16] In D_2O, vibrational frequencies shift, and $^1O_2$ energy transfer becomes less efficient.[16] Consistent with this, the intensity of the $^1O_2$ signal observed with δ-MnO_2 and H_2O_2 was almost 3.5-4.5 times higher in D_2O than that observed in H_2O with all other parameters being the same (tests #5 & #7). This confirms that SOSG emissions observed with H_2O_2 decomposition are in fact related to $^1O_2$. Furthermore, similar measurements probing N_3^--induced $^1O_2$ generation resulted in the dramatic decrease in the enhancement of SOSG intensity when H_2O instead of D_2O was used as the solvent (test #7). The SOSG signal increased only 1.5% with

View Article Online
DOI: 10.1039/D6CC01794K

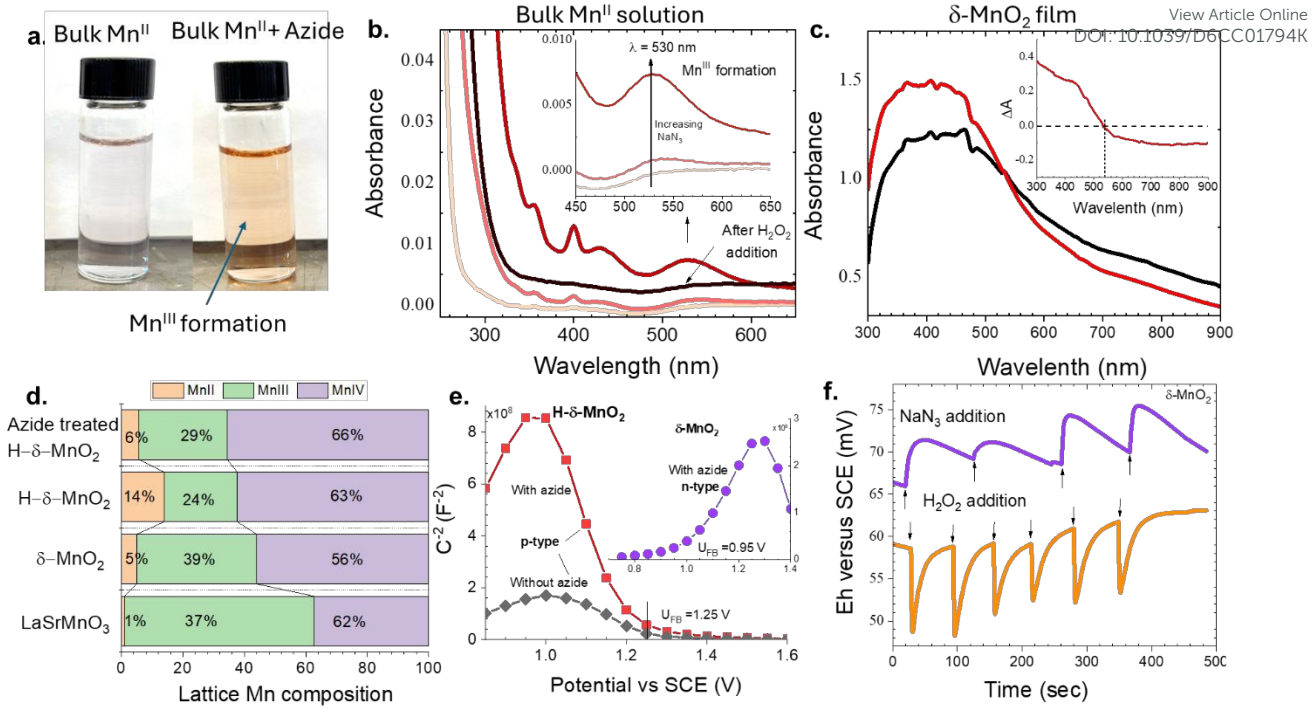

***Figure 2**. a&b) Photographs and absorption spectrum of bulk Mn^{II} solution with the addition of NaN_3; c) In-situ changes in the absorption spectrum of δ-MnO_2 due to NaN_3 addition; d) Comparison of lattice Mn cation composition of pristine and azide-treated Mn oxide powders obtained from PL spectroscopy; e) Mott Schottky plots of H-δ-MnO_2 and δ-MnO_2 (inset) in the presence/absence of azide; and f) Changes in the Eh (OCP) of δ-MnO_2 film upon sequential addition of 15 mM NaN_3 and then 10 μM of H_2O_2 pulses.*

H_2O_2 addition with H_2O as a solvent compared to 94% observed in D_2O. This is additional evidence for the $^1O_2$ formation.

Although SOSG tests confirmed the effect of azide-induced activation, the amount of $^1O_2$ produced could not be calculated due to the lack of information on the probe sensitivity factor. Hence, runs were performed using DPBF, a more well-studied probe[9]. The testing was also extended to $LiMn_2O_4$, La_2NiO_4, and $LaSrMnO_3$, and H-δ-MnO_2 that also good $^1O_2$ generators[8] to test the quenching/stimulating effects of N_3^-. **Figures 1b &1c** compare DPBF emission changes of the supernatant and $^1O_2$ produced for various oxides with and without the presence of azide. The results indicate that V_2O_5 followed by H-δ-MnO_2 are the most active catalysts for the disproportionation of H_2O_2 disproportionation to $^1O_2$ among the oxides tested in the ethanol/water mixture. The addition of azide again produces contrasting trends. In δ-MnO_2 and $LaSrMnO_3$ to a smaller extent **(Fig.1b & Fig.S1)**, NaN_3 addition stimulates $^1O_2$ generation, as seen from the dramatic decrease in emission intensity with increasing concentrations of H_2O_2 in the presence of azide. However, only a marginal decrease in emission intensity is observed with other oxides, such as La_2NiO_4 (**Fig.1b & Fig.S1**) and $LiMn_2O_4$ (**Fig.S1**). Thus, NaN_3 acts as a quencher for $^1O_2$ on these catalysts like that seen in V_2O_5. The quenching effects of NaN_3 in these catalysts compared to the stimulating effect seen in δ-MnO_2 indicates that the mere presence of Mn is not the cause of the contrasting effects. **Fig.1c** plots the $^1O_2$ concentration calculated from calibration curve and sensitivity factor[9] as a function of H_2O_2 concentration. The presence of azide leads to an increase in $^1O_2$ production only in δ-MnO_2. We also evaluated the effect of the composition of δ-MnO_2 on the stimulating effects of NaN_3. The acid treatment of δ-MnO_2 (H-δ-MnO_2) at pH =3 is known to increase the Mn^{II} and Mn vacancy concentrations in the lattice and switch in conductivity from n-type to p-type.[17] **Figs.1b&1c** show that, even in the absence of N_3^-, H-δ-MnO_2 has a higher catalytic activity for H_2O_2 to $^1O_2$ conversion than δ-MnO_2. In the presence of N_3^-, the $^1O_2$ is further enhanced, much more than that seen with δ-MnO_2. Therefore, the presence of Mn^{II}/vacancy leads to an enhancement of azide stimulation.

It is known that N_3^- can act as a bridging ligand by complexing with Mn^{II} ions in bulk to form coordination compounds, such as tri- and tetranuclear clusters.[18] Mn^{II}-azide complexes in bulk undergo a slow oxidation in air-saturated solutions to form the Mn^{III}-azide complex that has a visible absorption peak at 430 nm.[19, 20] We confirmed this by adding a 1-3 mM NaN_3 solution directly to air-saturated 0.1 M Mn^{II}SO$_4$ under ambient conditions. As shown in **Fig.2a**, the initially light pink solution of Mn^{II} turned into increasing shades of dark orange upon oxidation, which is characteristic of the Mn^{III}-azide complex. The absorbance spectrum (**Fig.2b**) shows a marked increase in visible light absorbance between 430-530 nm that increases with an increase in NaN_3 concentration (**Inset of Fig.2b**). This peak is characteristic of Mn^{III} complexes, such as Mn^{III}-pyrophosphate at 480 nm, and Mn^{III}-ethylenediaminetetraacetic acid at 464 nm, respectively.[21] Therefore, it is possible that the N_3^- can bind to the lattice Mn^{II} of δ-MnO_2 catalyst that after rapid oxidation in air forms a metastable Mn^{III}-azide complex that catalyses the disproportionation of H_2O_2 to $^1O_2$. To confirm this, we monitored *in-situ* the absorbance change of a δ-MnO_2 film with the addition of 15 mM of NaN_3 solution **(Fig.2c)**. The spectrum taken immediately after NaN_3 addition shows a marked increase in absorbance at wavelength less than 530 nm, as also evident in $\Delta A = A_{\partial-MnO_2,NaN_3} - A_{\partial-MnO_2}$ spectrum (inset), which provide clear evidence for lattice Mn^{III} formation. To understand why N_3^--induced $^1O_2$ enhancement is specific to δ-MnO_2, we analysed the lattice Mn cation composition of different MnO_x through X-ray photoelectron spectroscopy and photoluminescence spectroscopy (PL), as detailed elsewhere[22], and

is summarized in **Fig.S3** and **Fig.2d**. $LaSrMnO_3$ has the highest concentration of Mn^{III} (37%) and the lowest concentration of Mn^{II} (1%) in the lattice. Whereas δ-MnO_2 has the highest Mn^{II} content in its lattice (5%), which after acid treatment increases further to 14%. Given that H-δ-MnO_2 shows a higher enhancement in the N_3^--induced $^1O_2$ production than that seen in δ-MnO_2, the effect of N_3^- is likely correlated with the increased presence of Mn^{II} in the lattice. After azide treatment, the lattice Mn^{III} concentration of H-δ-MnO_2 increased from 24% to 29%, while the Mn^{II} concentration decreased from 14% to 6%. This is further confirmation that Mn^{II} after azide treatment is converted to Mn^{III}. The lower azide-induced $^1O_2$ production seen other MnO_x may be related to a fewer Mn^{II} lattice sites for azide complexation. The observation that azide-treated H-δ-MnO_2 is much more catalytic towards $^1O_2$ production than azide-treated δ-MnO_2 as well as $LaSrMnO_3$ with its high Mn^{III} content indicates that freshly formed surface Mn^{III} on a δ-MnO_2 structure is more active for H_2O_2 disproportionation. Note that when H_2O_2 was added to the bulk Mn^{III}-azide complex in the presence of SOSG (test #8, **Fig.1**) the intensity of $^1O_2$-related SOSG signal decreased rather than increased with H_2O_2 addition. Therefore, the bulk Mn^{III}-azide does not catalyse H_2O_2 disproportionation to $^1O_2$.

These different quenching/stimulating effects of azide on $^1O_2$ may be related to the differences in thermodynamic redox potential. The redox potential of $^1O_2/H_2O_2$ reaction, $U^0_{^1O_2/H_2O_2}$, is 0.77 V versus the standard hydrogen electrode (SHE) at pH = 7 for H_2O_2 and $^1O_2$ concentrations of 10 μM. The redox potential of $Mn^{III}-N_3^-/Mn^{II}-N_3^-$ complex in the bulk is only 0.66 V[23] and therefore, cannot induce H_2O_2 disproportionation to $^1O_2$, as observed here. On the other hand, V_2O_5, δ-MnO_2 and H-δ-MnO_2 are known to be semiconductors with high work function and electron affinity values (5.6-6 eV),[17, 24] which is also influenced by different ligands in the electrolyte.[17, 21] The flat band potential (U_{FB}) determined from the Mott-Schottky (M-S) plots (**Fig.2e**) of δ-MnO_2 and H-δ-MnO_2 are 1.2 V and 1.5 V versus SHE, respectively, with the former and the latter being n-type and p-type semiconductors, respectively. These U_{FB} values are more positive than $U^0_{^1O_2/H_2O_2}$, which explains why both materials have a high catalytic activity for $^1O_2$ production from H_2O_2. In the presence of azide, the bulk U_{FB} does not shift significantly, indicating that azide does not modulate the bulk electronics properties. However, its addition leads to a positive shift in the oxidation-reduction potential (Eh, **Fig.2f**) or open circuit potential (OCP), which is more reflective of the surface Fermi level (E_F) changes.[25] This Eh value corresponds to the relative difference between the surface potential of δ-MnO_2, equivalent to E_F under band bending conditions, and the reference electrode.[25] The concomitant increase in the lattice Mn^{III} content suggests that the Mn^{III} formation causes a decrease in the surface E_F position, thus producing an even greater driving force for e^- injection from $^1O_2/H_2O_2$ reaction. Mn^{III} is also the active site for H_2O oxidation.[26] Consistent with this, the addition of H_2O_2 to the aqueous azide solution in contact with δ-MnO_2 results in a negative shift in Eh, implying an increase in the surface E_F position. This is as expected since e^- injection would lead to an increase in E_F energy and a conversion of Mn^{III} to back to Mn^{II} (**Fig.2b**).

In summary, this study reports an unusual improvement in the efficiency of H_2O_2 disproportionation on δ-MnO_2 to $^1O_2$ in the presence of NaN_3, which paradoxically is a known $^1O_2$ quencher in bulk solution for most other catalysts. This activation is shown to be due to N_3^- complexation with lattice Mn^{II} of δ-MnO_2 that upon rapid air oxidation, produces a metastable surface Mn^{III}-azide complex that strongly catalyses H_2O_2 disproportionation under neutral conditions.

ACKNOWLEDGEMENTS

View Article Online
DOI: 10.1039/D6CC01794K

The authors are grateful for financial support provided by the Howard P. Isermann fellowship and the Rensselaer Polytechnic Institute.

Conflict of Interest

All authors declare that they have no conflicts of interest.

DATA AVAILABILITY

The data supporting this article have been included as part of the Supplementary Information. Supplementary information: Emission spectrum, calibration curves, and experimental details.

REFERENCES

1. J. Tang, J. Chen, Z. Zhang, Q. Ma, X. Hu, P. Li, Z. Liu, P. Cui, C. Wan, Q. Ke, L. Fu, J. Kim, T. Hamada, Y. Kang and Y. Yamauchi, *Chem. Sci.*, 2023, **14**, 13402-13409.
2. J. R. Harbour and S. L. Issler, *J. Am. Chem. Soc.*, 1982, **104**, 903-905.
3. C. Schweitzer and R. Schmidt, *Chem. Rev.*, 2003, **103**, 1685-1758.
4. W. R. Haag and T. Mill, *Photochem. Photobiol.*, 1987, **45**, 317-321.
5. N. Miyoshi, M. Ueda, K. Fuke, Y. Tanimoto, M. Itoh and G. Tomita, *Zeitschrift für Naturforschung B*, 1982, **37**, 649-652.
6. M. Li, C. S. Cline, E. B. Koker, H. H. Carmichael, C. F. Chignell and P. Bilski, *Photochem. Photobiol.*, 2001, **74**, 760-764.
7. M. A. Rubio, D. O. Mártire, S. E. Braslavsky and E. A. Lissi, *J. Photochem. Photobiol. A: Chem.*, 1992, **66**, 153-157.
8. S. Mangu and V. Chakrapani, *J. Phys. Chem. C*, 2026, **130**, 6180–6191.
9. T. Entradas, S. Waldron and M. Volk, *J. Photochem. Photobiol. B, Biol.*, 2020, **204**, 111787.
10. X. Ragàs, A. Jiménez-Banzo, D. Sánchez-García, X. Batllori and S. Nonell, *Chem. Commun.*, 2009, DOI: 10.1039/b822776d, 2920-2922.
11. H. Liu, P. J. Carter, A. C. Laan, R. Eelkema and A. G. Denkova, *Sci. Rep.*, 2019, **9**, 8393.
12. F. Natalio, R. André, A. F. Hartog, B. Stoll, K. P. Jochum, R. Wever and W. Tremel, *Nat. Nanotechnol.*, 2012, **7**, 530-535.
13. S. Lee, Q. Wang and V. Chakrapani, *Phys. Rev. Mater.*, 2024, **8**, 125801.
14. V. Chakrapani, M. Brier, A. Puntambekar and T. DiGiovanni, *J. Mater. Res. Focus Issue Early Career Scholar in Material Science*, 2016, ***31***, 17.
15. N. Miyoshi, M. Ueda, K. Fuke, Y. Tanimoto, M. Itoh and G. Tomita, *Z. Naturforsch. B*, 1982, **37**, 649-652.
16. P. B. Merkel and D. R. Kearns, *J. Am. Chem. Soc.*, 1972, **94**, 7244-7253.
17. C. Wang, N. Smieszek and V. Chakrapani, *Chem. Mater.*, 2021, **33**, 7805-7817.
18. M. Shee and N. P. Singh, *Chem. Soc. Rev.*, 2022, **51**, 2255-2312.
19. H. D. Moya, E. A. Neves, M. E. Vázquez and N. Coichev, *Talanta*, 1996, **43**, 67-72.
20. H. D. Moya, E. A. Neves and N. Coichev, *Spectroscopy Letters*, 2001, **34**, 537-547.
21. C. Wang and V. Chakrapani, *ACS Earth Space Chem.*, 2023, **7**, 774-787.
22. V. Chakrapani, C. Wang, Q. Wang and N. Smieszek, *Surf. Interface Anal.*, 2022, **54**, 1192-1202.
23. H. D. Moya, E. A. Neves and N. Coichev, *Talanta*, 1997, **44**, 797-803.

View Article Online
DOI: 10.1039/D6CC01794K

24. S. Lee, Q. Wang and V. Chakrapani, *J. Appl. Phys.* , 2024, **136**, 205101.
25. V. Chakrapani, in *Metal Ions and the Route to Life*, eds. W. Nitschke and S. Duval, CRC Press, Boca Raton, 1st edn., 2025, DOI: 10.1201/9781003459910-7, p. 24.
26. I. Roy, C. Wang, N. Smieszek, X. Li, L. Tsapatsaris and V. Chakrapani, *ChemSusChem*, 2022, **15**, e202200062.

View Article Online
DOI: 10.1039/D6CC01794K

DATA AVAILABILITY

The data supporting this article have been included as part of the Supplementary Information. Supplementary information: Emission spectrum, Calibration curves and further experimental details.